NASA/TM—202300000000

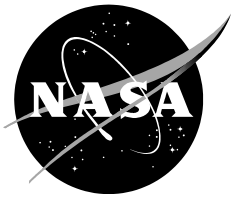

TESS Data Release Notes:
Sector 67, DR94

Christopher J. Burke
Kavli Institute for Astrophysics and Space Science, Massachusetts Institute of Technology, Cambridge, Massachusetts

Michael M. Fausnaugh
Texas Tech University, Lubbock, Texas

Douglas A. Caldwell
SETI Institute, Mountain View, California

Jon M. Jenkins
NASA Ames Research Center, Moffett Field, California

Joseph D. Twicken
SETI Institute, Mountain View, California

Roland Vanderspek
Kavli Institute for Astrophysics and Space Science, Massachusetts Institute of Technology, Cambridge, Massachusetts

Eric B. Ting
NASA Ames Research Center, Moffett Field, California

Stephanie Striegel
SETI Institute, Mountain View, California

Rebekah Hounsell
University of Maryland Baltimore County, Baltimore, Maryland
NASA Goddard Space Flight Center, Greenbelt, Maryland

October 2, 2023

NASA STI Program ... in Profile

Since its founding, NASA has been dedicated to the advancement of aeronautics and space science. The NASA scientific and technical information (STI) program plays a key part in helping NASA maintain this important role.
The NASA STI program operates under the auspices of the Agency Chief Information Officer. It collects, organizes, provides for archiving, and disseminates NASA's STI. The NASA STI program provides access to the NTRS Registered and its public interface, the NASA Technical Reports Server, thus providing one of the largest collections of aeronautical and space science STI in the world. Results are published in both non-NASA channels and by NASA in the NASA STI Report Series, which includes the following report types:

- TECHNICAL PUBLICATION. Reports of completed research or a major significant phase of research that present the results of NASA Programs and include extensive data or theoretical analysis. Includes compilations of significant scientific and technical data and information deemed to be of continuing reference value. NASA counterpart of peer-reviewed formal professional papers but has less stringent limitations on manuscript length and extent of graphic presentations.
- TECHNICAL MEMORANDUM.
  Scientific and technical findings that are preliminary or of specialized interest, e.g., quick release reports, working papers, and bibliographies that contain minimal annotation. Does not contain extensive analysis.
- CONTRACTOR REPORT. Scientific and technical findings by NASA-sponsored contractors and grantees.
- CONFERENCE PUBLICATION.
  Collected papers from scientific and technical conferences, symposia, seminars, or other meetings sponsored or co-sponsored by NASA.
- SPECIAL PUBLICATION.
  Scientific, technical, or historical information from NASA programs, projects, and missions, often concerned with subjects having substantial public interest.
- TECHNICAL TRANSLATION.
  English-language translations of foreign scientific and technical material pertinent to NASA's mission.

Specialized services also include organizing and publishing research results, distributing specialized research announcements and feeds, providing information desk and personal search support, and enabling data exchange services.

For more information about the NASA STI program, see the following:

- Access the NASA STI program home page at http://www.sti.nasa.gov
- E-mail your question to help@sti.nasa.gov
- Phone the NASA STI Information Desk at 757-864-9658
- Write to:
  NASA STI Information Desk
  Mail Stop 148
  NASA Langley Research Center
  Hampton, VA 23681-2199

NASA/TM—202300000000

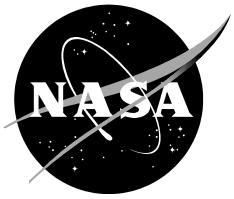

TESS Data Release Notes:
Sector 67, DR94

Christopher J. Burke
Kavli Institute for Astrophysics and Space Science, Massachusetts Institute of Technology, Cambridge, Massachusetts

Michael M. Fausnaugh
Texas Tech University, Lubbock, Texas

Douglas A. Caldwell
SETI Institute, Mountain View, California

Jon M. Jenkins
NASA Ames Research Center, Moffett Field, California

Joseph D. Twicken
SETI Institute, Mountain View, California

Roland Vanderspek
Kavli Institute for Astrophysics and Space Science, Massachusetts Institute of Technology, Cambridge, Massachusetts

Eric B. Ting
NASA Ames Research Center, Moffett Field, California

Stephanie Striegel
SETI Institute, Mountain View, California

Rebekah Hounsell
University of Maryland Baltimore County, Baltimore, Maryland
NASA Goddard Space Flight Center, Greenbelt, Maryland

October 2, 2023

Acknowledgements

These Data Release Notes provide information on the processing and export of data from the Transiting Exoplanet Survey Satellite (TESS). The data products included in this data release are full frame images (FFIs), target pixel files, light curve files, collateral pixel files, cotrending basis vectors (CBVs), and Data Validation (DV) reports, time series, and associated xml files.

These data products were generated by the TESS Science Processing Operations Center (SPOC, Jenkins et al., 2016) at NASA Ames Research Center from data collected by the TESS instrument, which is managed by the TESS Payload Operations Center (POC) at Massachusetts Institute of Technology (MIT). The format and content of these data products are documented in the Science Data Products Description Document (SDPDD)[1]. The SPOC science algorithms are based heavily on those of the Kepler Mission science pipeline, and are described in the Kepler Data Processing Handbook (Jenkins, 2020).[2] The Data Validation algorithms are documented in Twicken et al. (2018) and Li et al. (2019). The TESS Instrument Handbook (Vanderspek et al., 2018) contains more information about the TESS instrument design, detector layout, data properties, and mission operations.

The TESS Mission is funded by NASA's Science Mission Directorate.

This report is available in electronic form at
https://archive.stsci.edu/tess/

[1] https://archive.stsci.edu/missions/tess/doc/EXP-TESS-ARC-ICD-TM-0014-Rev-F.pdf
[2] https://archive.stsci.edu/kepler/manuals/KSCI-19081-003-KDPH.pdf

1 Observations

TESS Sector 67 observations include physical orbits 141 and 142 of the spacecraft around the Earth. Data collection was paused for a total of 0.63 days to download data. Data were downloaded approximately every seven days, near apogee and perigee of each orbit. In total, there are 27.1 days of science data collected in Sector 67.

Table 1: Sector 67 Observation times

	UTC	TJD[a]	Cadence #
Orbit 141a start	2023-07-01 03:14:33	3126.63659	1367411
Orbit 141a end	2023-07-07 14:42:33	3133.11436	1372075
Orbit 141b start	2023-07-07 19:44:33	3133.32409	1372226
Orbit 141b end	2023-07-14 17:56:33	3140.24908	1377212
Orbit 142a start	2023-07-14 23:00:33	3140.46019	1377364
Orbit 142a end	2023-07-22 04:52:32	3147.70464	1382580
Orbit 142b start	2023-07-22 09:54:32	3147.91436	1382731
Orbit 142b end	2023-07-28 21:26:32	3154.39491	1387397

[a] TJD = TESS JD = JD - 2,457,000.0

[b]The horizontal black lines mark gaps in the light curves for data downlink.

The spacecraft was pointing at RA (J2000): 326.77°; Dec (J2000): −74.28°; Roll: −142.53°. See the TESS project Sector 67 observation page[3] for the coordinates of the spacecraft pointing and center field-of-view of each camera. Fields-of-view for each camera can be found at the TESS Guest Investigator Office observations status page.[4] Grayscale images for each camera and CCD along with RA and Declination coordinates are shown in Figure 1. Additional details for Guest Investigator target lists selected for 2-minute and 20-second observations can be found at the Sector 67 observation page and the observations status page.

1.1 Targets and Light Curves

There were 2263 targets chosen for 20-second cadence observations and 13000 targets chosen for 2-minute cadence observations. Table 2 provides targets that were not fully processed with the photometric pipeline as well as targets that were fully processed but received warnings during aperture assignment.

For targets that were not processed with the photometric pipeline, the target pixel files with original and calibrated pixel data are provided, but no light curves are produced. Note that the target pixel files do not include a background correction for stars without light curves. The most common reason for a target to not be processed with the photometric pipeline is that the target exceeds a brightness threshold (Tmag $\lesssim$ 1.8) that results in large pixel stamps. A target located too close to a very bright star, having a comparably bright companion, impacted by saturated star bleed trails, or having an error in identifying

[3] https://tess.mit.edu/observations/sector-67

[4] https://heasarc.gsfc.nasa.gov/docs/tess/sector.html

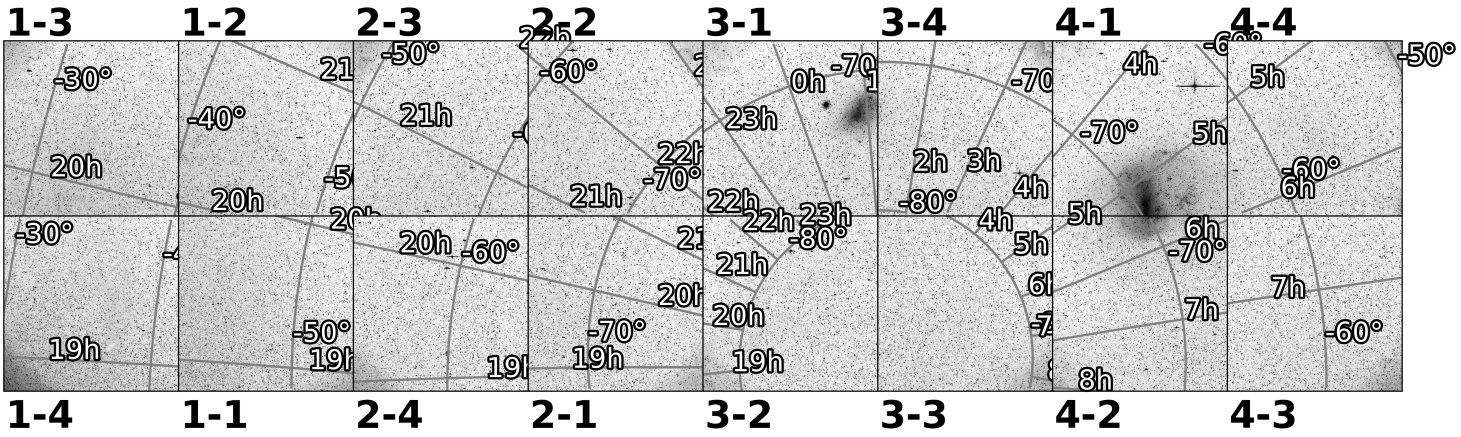

Figure 1: Grayscale TESS image for each camera and ccd (format camera#-ccd#) as labeled next to each panel. Inverse scaling (dark represents brighter image flux and light represents darker image flux) is used. Grid lines represent RA and Declination.

a clean background region are less common causes for a target to not be processed with the photometric pipeline. Visual examination of the target along with custom aperture selection may be needed for photometric analysis of the impacted targets. Warnings during aperture assignment occur when the aperture is discontinuous or clipped, and the resulting photometry is expected to be unreliable.

Table 2: TIC Ids for targets with missing light curves and photometric aperture warnings

Missing Light Curve		Aperture Warning	
2-minute	20-second	2-minute	20-second
38877693		230979227	267211065
238196512		254125171	
		267211065	
		300015238	
		514062507	
		612256219	

1.2 Spacecraft Pointing and Momentum dumps

The pointing in Sector 67 was set at −55.5 degrees in ecliptic latitude. Camera 1 and Camera 4 were both used for guiding in Orbit 141a and 142a, while Camera 4 alone was used for guiding in Orbit 141b and 142b. Two momentum dumps were performed in each orbit. The momentum dumps are performed at the end of each data downlink just before data collection resumes. Data impacted by momentum dumps and data downlinks are marked with data quality flags (see Appendix A). Figure 2 summarizes the pointing performance over the course of the sector based on Fine Pointing telemetry.

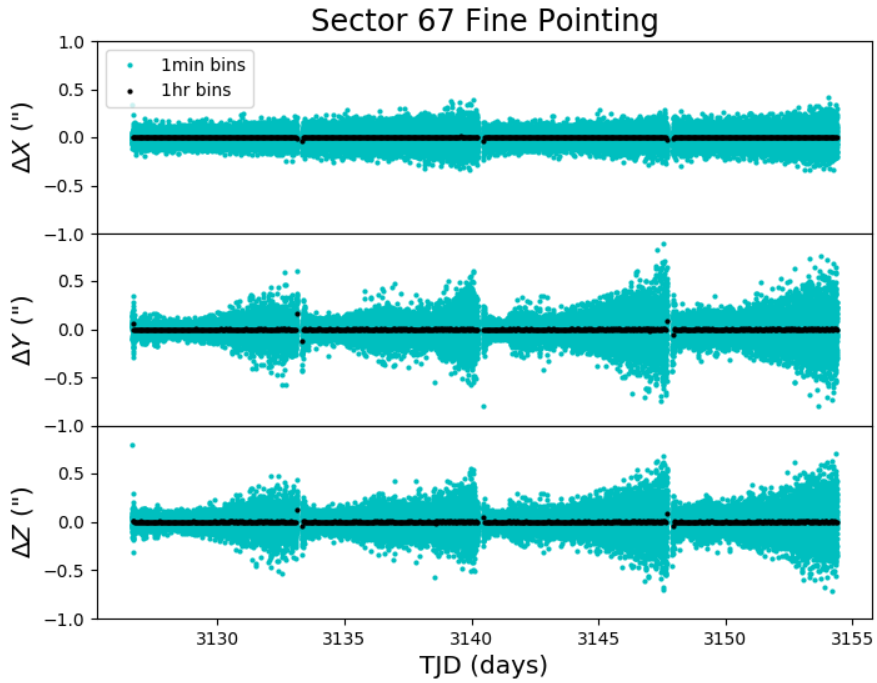

Figure 2: The delta-quaternions from each camera have been converted to spacecraft frame, binned to 1 minute and 1 hour. Long-term trends (such as those caused by differential velocity aberration) have also been removed. The ΔX/ΔY directions represent offsets along the detectors' rows/columns, while the ΔZ direction represents spacecraft roll.

1.3 Scattered Light

Figure 3 shows the median value of the background estimate for all targets on a given CCD as a function of time. Times of high background correspond to times when the Earth and/or Moon approach the camera's field of view causing scattered light from these bright objects to enter the cameras. The viewing geometry of the Earth and Moon relative to TESS's pointing in Sector 67 are shown in Figure 4. Figure 4 shows the angle between each camera's boresight and the Earth or Moon—this figure can be used to identify periods affected by scattered light and the relative contributions of the Earth and Moon to the image backgrounds. Scattered light increases as the camera boresight angle between the Earth and Moon is $\lesssim 35°$ and will strongly impact photometric observations for angles $\lesssim 25°$. Data impacted by scattered light are marked with data quality flags (see Appendix A). As shown in Figures 3 and 4, in Sector 67, the Earth introduces scattered light signals at the end of each orbit, and the Moon strongly impacts Camera 1 at the end of Orbit 142.

1.4 Smear Correction Contamination

Due to the shutterless operation of the TESS instrument (see TESS Instrument Handbook, §9.5), data calibration involves subtracting a smear correction. The "smear rows" are virtual pixels (not physical pixels) that provide an estimate of the contaminating flux that accumu-

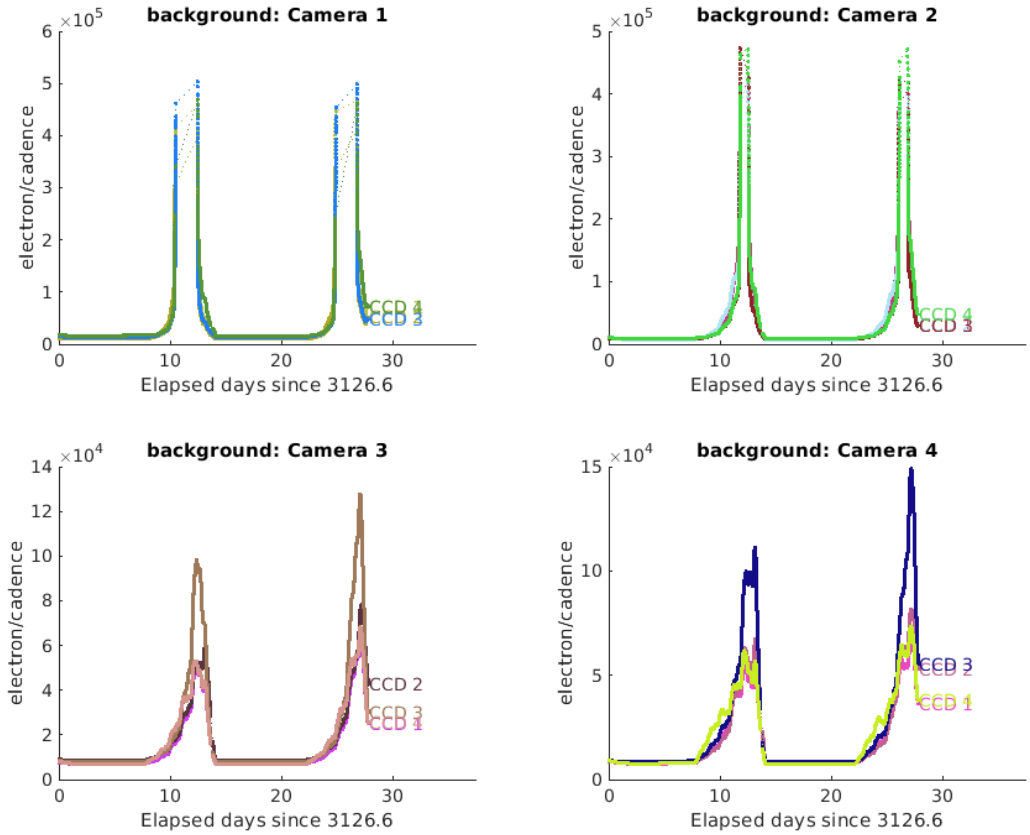

Figure 3: Median background flux across all targets on a given CCD in each camera. The changes are caused by variations in the orientation and distance of the Earth and Moon.

lates in each pixel during the rapid (∼0.02s) shutterless frame transfer. The smear correction, estimated from the smear rows, is subtracted from the whole column. However, bright stars located in the science frame, upper buffer rows, and lower science frame rows can bleed into the smear row resulting in an overestimated smear correction. An overestimated smear correction in calibrated data products can be identified by one or more consecutive columns that are anomalously dark relative to neighboring columns, whereas the raw/uncalibrated images do not reveal an anomalously dark column relative to its neighbors. Mitigating an overestimated smear correction may require a custom calibration that robustly interpolates across the contaminated smear columns or a robust smear estimate from the science frame.

The columns listed in Table 3 were impacted by bright stars in the science frame, and/or upper buffer rows, and/or lower science frame rows, which bleed into the upper serial register resulting in an overestimated smear correction.

1.5 Data Anomaly Flags

The SDPDD (§9) lists data quality flags and the associated binary values used for TESS data. Appendix A describes each Data Anomaly Flag in more detail.

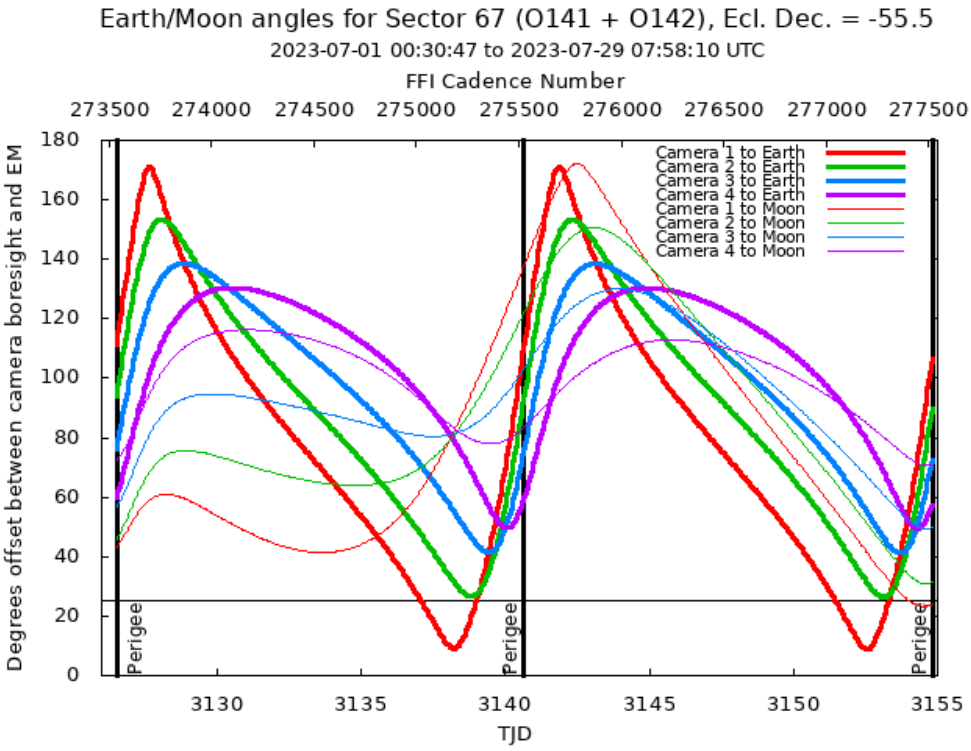

Figure 4: Angle between the four camera boresights and the Earth/Moon as a function of time. When the Earth is within $\sim 25°$ of a camera's boresight, transiting planet searches may be compromised by high levels of scattered light. At larger angles, up to $\sim 35°$, scattered light patterns and complicated structures may be visible. At yet larger angles, low level patchy features may be visible. Scattered light from the Moon is generally only noticeable below $\sim 35°$. This figure can be used to identify periods affected by scattered light and the relative contributions of the Earth and Moon to the background. However, the background intensity and locations of scattered light features depend on additional factors, such as the Earth/Moon azimuth and distance from the spacecraft.

2 Pipeline Performance and Results

2.1 Light Curves and Photometric Precision

Figure 5 shows an assessment of the PDC systematic error correction of the pipeline by comparing simple aperture photometry light curves from PA and the PDC contrended light curves. Figure 6 shows the achieved Combined Differential Photometric Precision (CDPP) at 1-hour timescales for all two-minute targets.

We encourage users to examine several light curve quality assessment values (CROWDSAP, PDC_TOT, PDC_COR, and PDC_NOI) that are available in the light curve data product fits headers; in particular, in the second fits header of light curve data products (see SDPDD).

The CROWDSAP keyword represents the fraction of flux in the photometric aperture attributable to the target star (after background correction). A low value for CROWDSAP indicates that other stars contribute a significant amount of flux to the target and the light

Table 3: Columns Impacted by Smear Correction Contamination

Camera	CCD	Column
1	1	1659
1	3	578
3	1	1504
3	2	401
3	2	550
3	2	888
3	2	1827
4	3	1586
4	4	737
4	4	1201

curve may not isolate variability for the target star of interest.

The keywords PDC_TOT, PDC_COR, and PDC_NOI assess the quality of the PDC cotrending procedure. Values of the PDC keywords range from 0.0 to 1.0, with values towards 1.0 indicating a high quality of the PDC cotrending outcome (KDPH; §8.3.3.XIV). The correlation goodness metric (PDC_COR), is calibrated such that a value greater than 0.8 means there is less than 10% mean absolute correlation between the target under study and all other targets on the CCD. The introduced noise metric (PDC_NOI) is calibrated such that a value greater than 0.8 means the power in broad-band introduced noise is below the level of uncertainties in the flux values. The total goodness metric (PDC_TOT) provides an overall summary of the cotrending quality.

2.2 Transit Search and Data Validation

In Sector 67, the two-minute light curves of 12998 targets were subjected to the transit search in TPS. Of these, Threshold Crossing Events (TCEs) at the 7.1 σ level were generated for 949 targets.

We employed an iterative method when conducting the Sector 67 transit search. The top panel of Figure 7 shows the number of TCEs at a given cadence that exhibit a transit signal from an initial run of TPS. The 3-σ peaks were used to define de-emphasis weights for a second run of TPS, the results of which are shown in the bottom panel of Figure 7. The final set of TCEs and the results reported here are based on the second run of TPS. The values of the adopted de-emphasis weights are provided in the DV timeseries data products for targets with TCEs.

The top panel of Figure 8 shows the distribution of orbital periods for the final set of TCEs found in Sector 67. The bimodal nature of the period distribution is due to a large number of two-transit detections with periods ranging from 8 to 20 days, many of which are likely false positives. Two-transit TCEs can be identified with the `NTRANS` keyword in the headers of the dv-timeseries FITS files. The vertical histogram in the right panel of Figure 8 shows the distribution of transit depths derived from limb-darkened transiting planet model fits for TCEs. The model transit depths range down to the order of 100 ppm, but the bulk

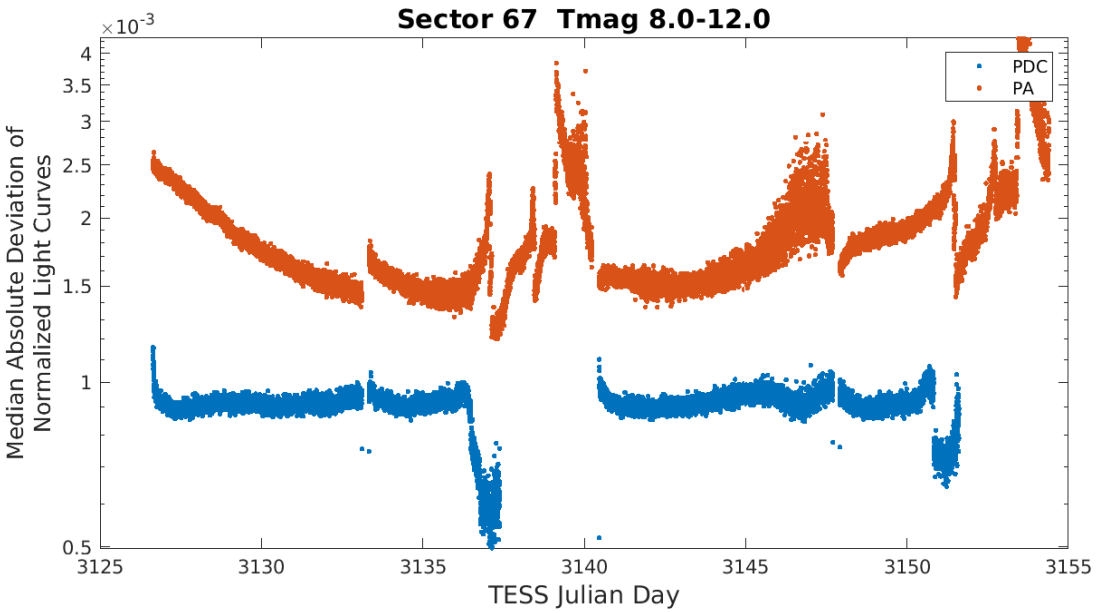

Figure 5: Median absolute deviation (MAD) for the two-minute cadence data from Sector 67, showing the performance of the cotrending after identifying Manual Exclude data quality flags. The MAD is calculated in each cadence across stars with flux variations less than 1% for both the PA (red) and PDC (blue) light curves, where each light curve is normalized by its median flux value. The scatter in the PA light curves is much higher than that for the PDC light curves, and the outliers in the PA light curves are largely absent from the PDC light curves due to the use of the anomaly flags.

of the transit depths are considerably larger.

A search for additional TCEs in potential multiple planet systems was conducted in DV through calls to TPS. A total of 1340 TCEs were ultimately identified in the SPOC pipeline on 949 unique target stars. Table 4 provides a breakdown of the number of TCEs by target. Note that targets with large numbers of TCEs are likely to include false positives.

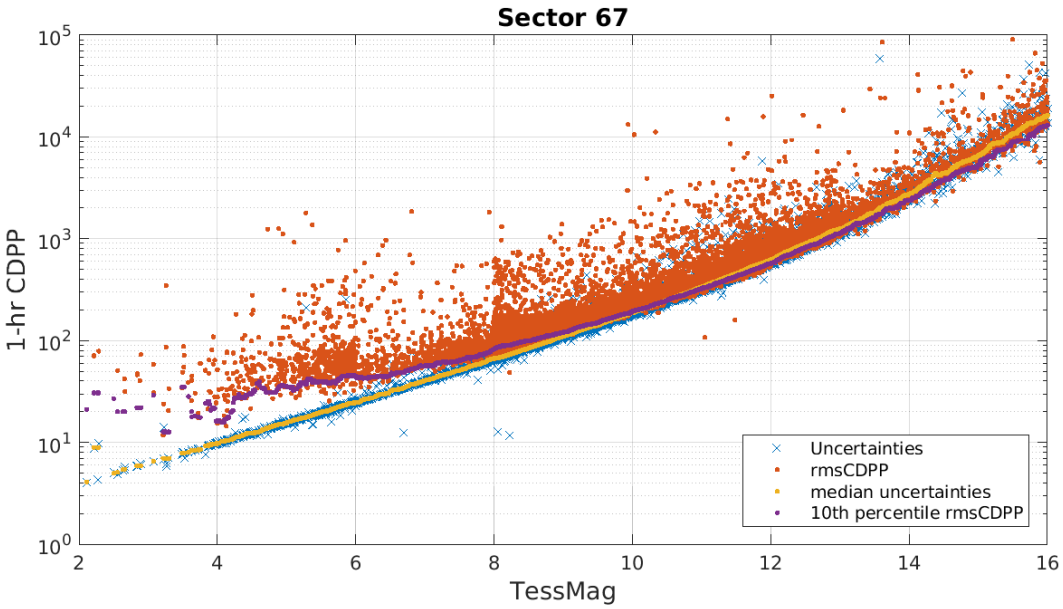

Figure 6: 1-hour CDPP. The red points are the RMS CDPP measurements for the 12998 light curves from Sector 67 plotted as a function of TESS magnitude. The blue x's are the uncertainties, scaled to 1-hour timescale. The purple curve is a moving 10th percentile of the RMS CDPP measurements, and the gold curve is a moving median of the 1-hr uncertainties.

Table 4: Sector 67 TCE Numbers

Number of TCEs	Number of Targets	Total TCEs
1	640	640
2	249	498
3	44	132
4	11	44
5	4	20
6	1	6
–	949	1340

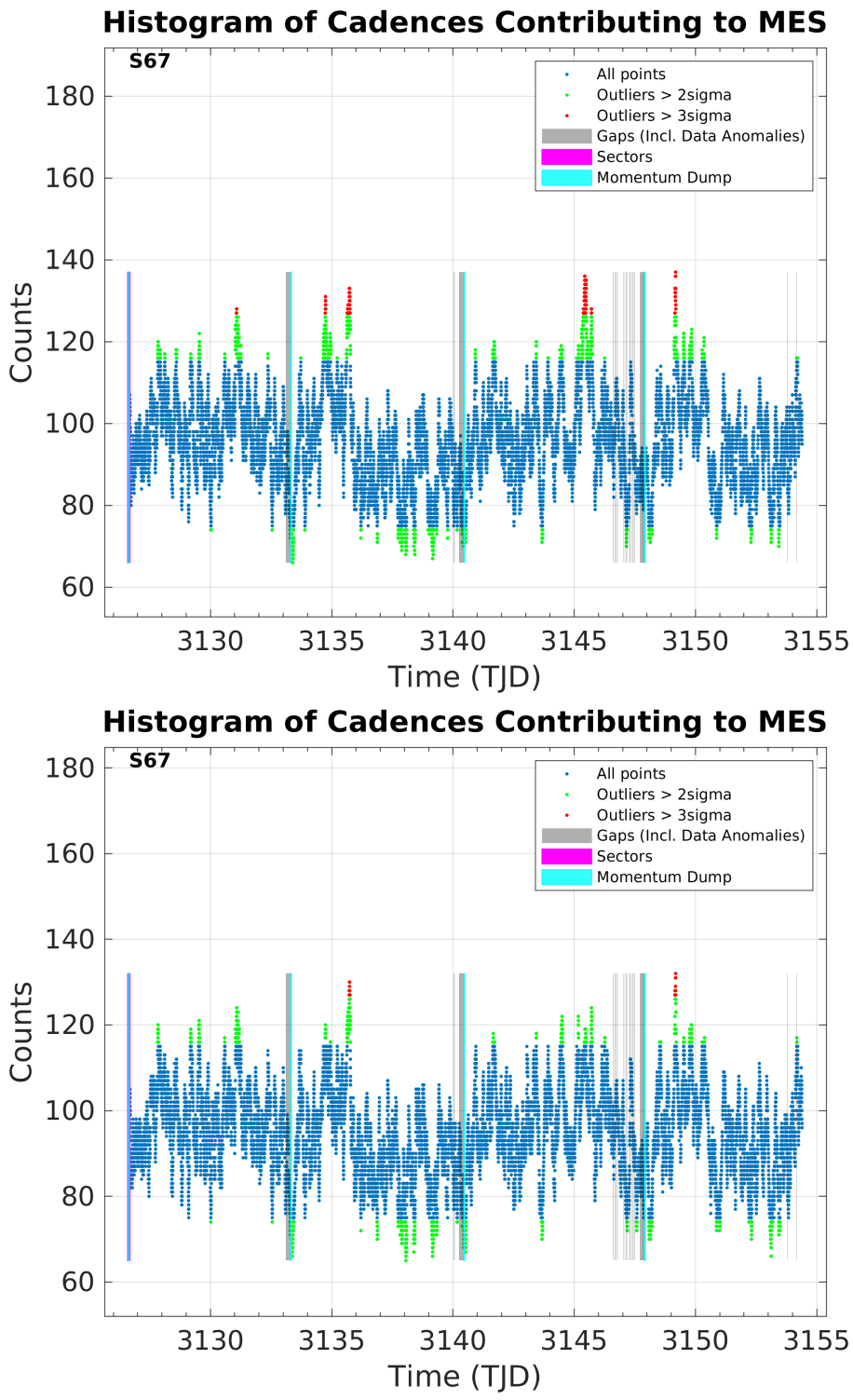

Figure 7: Top panel: Number of TCEs at a given cadence exhibiting a transit signal, based on an initial run of TPS. Any isolated peaks are caused by single events that result in spurious TCEs. These peaks were used to define de-emphasis weights that suppress problematic epochs for the transit detection statistics in a second iteration of TPS. Bottom panel: Results from the second run of TPS.

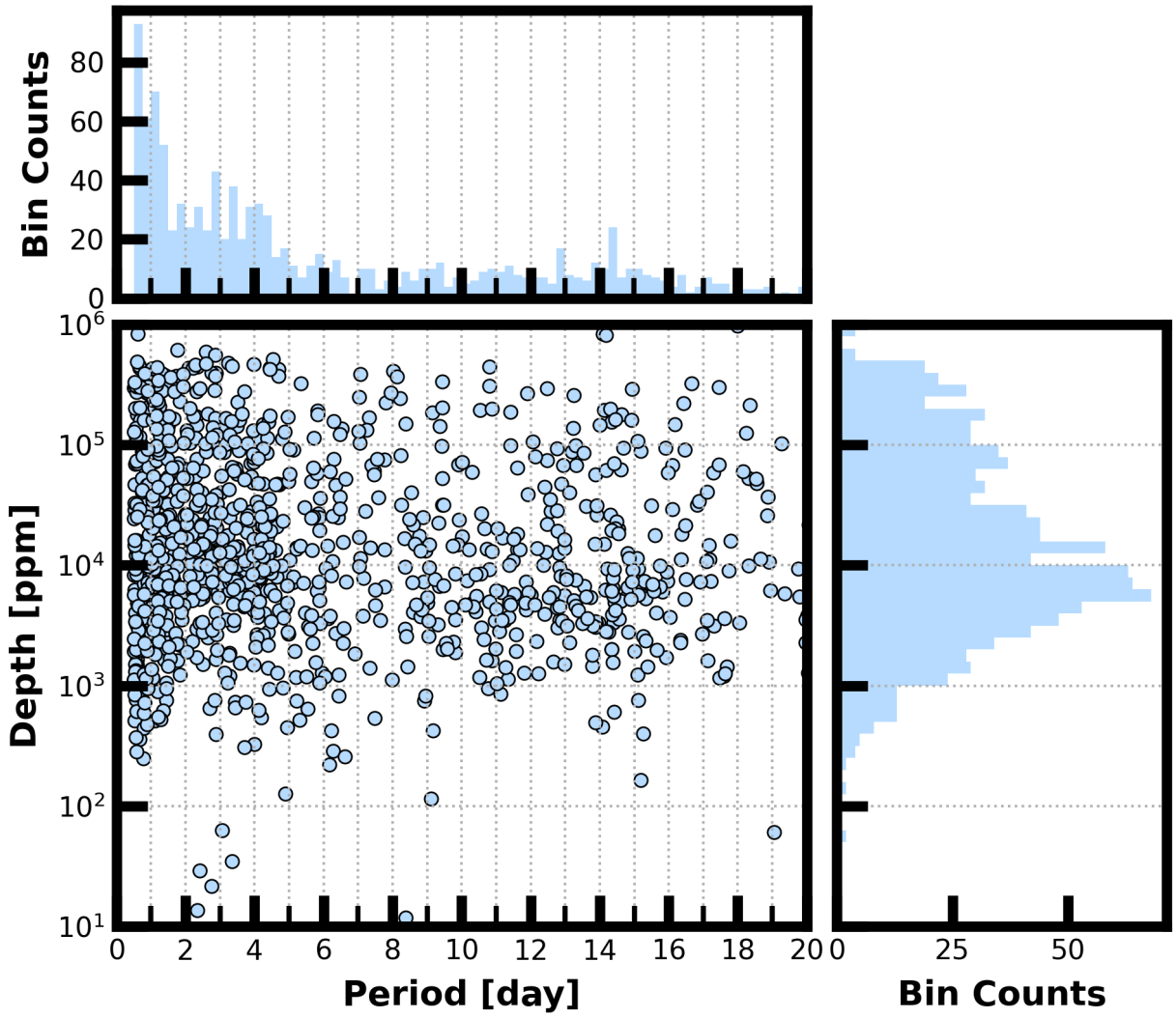

Figure 8: Lower Left Panel: Transit depth as a function of orbital period for the 1340 TCEs identified for the Sector 67 search. For enhanced visibility of long period detections, TCEs with orbital period <0.5 days are not shown. Reported depth comes from the DV limb-darkened transit fit depth when available, and the DV trapezoid model fit depth when not available. Top Panel: Orbital period distribution of the TCEs shown in the lower left panel. Right Panel: Transit depth distribution for the TCEs shown in the lower left panel.

Appendix A: Details of Data Anomaly Flags

See the SDPDD (§9) for a list of data quality flags and the associated binary values used for TESS data.

The following flags are set by hand, based on mission operations and spacecraft telemetry: bits 1 and 2 (Attitude Tweak and Safe Mode).

Cadences marked with bits 3, 4, 6, and 12 (Coarse Point, Earth Point, Reaction Wheel Desaturation Event, and Predicted Straylight) are flagged based on spacecraft telemetry. Cadences marked with bits 2 and 4 (Safe Mode and Earth Point) have `NULL` values for the timestamps and data in the target-pixel files and light curve files.

Note that just after the data downlinks near apogee (midpoint of each orbit), the spacecraft pointing is still settling for 20 to 60 seconds after data collection resumes. Cadences during this time are marked with bit 8 (Manual Exclude, described below).

Cadences marked with bit 5 and 10 (Argabrightening Events and Impulsive Outlier) were identified by the SPOC pipeline. Bit 5 marks a sudden change in the background measurements. In practice, bit 5 flags are caused by rapidly changing glints and unstable pointing at times near momentum dumps. Bit 10 marks an outlier identified by PDC and omitted from the cotrending procedure.

The 20-second data mode includes cadences marked with bit 7 and 11 (Cosmic Ray in Optimal Aperture and Cosmic Ray in Collateral Pixel). These flags indicate cadences affected by cosmic rays that are removed by the pipeline, and can be found in both the TPF and LC files. The data provided in the archive products are corrected for cosmic rays, and a `FITS` table extension in the TPF and Collateral Pixel File details the cosmic rays identified and removed by the pipeline at the pixel level.

Cadences marked with bit 8 (Manual Exclude) are ignored by PDC, TPS, and DV for cotrending and transit searches. These cadences were identified using spacecraft telemetry from the fine pointing system. All cadences with pointing excursions >7 arcsec (0.3 pixel) were flagged for manual exclude. These cadences can also be set manually in order to identify off-nominal data collection (e.g., engineering tests, spacecraft anomalies, etc).

The predicted stray light flag (bit 12, value 2048) is marked in the FFIs and flags times when the Earth/Moon are near the camera FOVs and may interfere with guiding or saturate the detectors. We strongly recommend that users inspect the FFI data before removing images marked with bit 12, as this flag is set based on predictions from mission planning and is known to be conservative with respect to the quality of data usable for analysis. This flag is disabled for the 2-minute and 20-second data products.

The scattered light exclude flag (bit 13, value 4096) identifies cadences at which individual targets are affected by scattered light.

If the Earth/Moon interference is strong enough to saturate the detector, all targets on a CCD slice will be affected and the data are unusable. Cadences with bad calibrations due to saturation are now explicitly marked with bit 15 (value 16384, "Bad Calibration Exclude"). For some cadences, the majority of targets on a CCD may be flagged for scattered light and not enough valid data remains to derive cotrending basis vectors in PDC. No systematic error correction can be applied at these times. This situation is identified by bit 16 (value 32768, "Insufficient Targets for Error Correction Exclude").

FFIs were only marked with bits 3, 4, 6, 8, 12, and 15 (Coarse Point, Earth Point,

Reaction Wheel Desaturation Events, Manual Exclude, Straylight, and Bad Calibration Exclude). There are no WCS coordinates for FFIs that coincide with momentum dumps (bit 6).

References

Jenkins, J. M. 2020, Kepler Data Processing Handbook: Overview of the Science Operations Center, Tech. rep., NASA Ames Research Center

Jenkins, J. M., Twicken, J. D., McCauliff, S., et al. 2016, in Proc. SPIE, Vol. 9913, Software and Cyberinfrastructure for Astronomy IV, 99133E, doi: 10.1117/12.2233418

Li, J., Tenenbaum, P., Twicken, J. D., et al. 2019, *PASP*, 131, 024506, doi: 10.1088/1538-3873/aaf44d

Twicken, J. D., Catanzarite, J. H., Clarke, B. D., et al. 2018, *PASP*, 130, 064502, doi: 10.1088/1538-3873/aab694

Vanderspek, R., Doty, J., Fausnaugh, M., et al. 2018, TESS Instrument Handbook, Tech. rep., Kavli Institute for Astrophysics and Space Science, Massachusetts Institute of Technology

Acronyms and Abbreviation List

BTJD Barycentric-corrected TESS Julian Date

CAL Calibration Pipeline Module

CBV Cotrending Basis Vector

CCD Charge Coupled Device

CDPP Combined Differential Photometric Precision

COA Compute Optimal Aperture Pipeline Module

CSCI Computer Software Configuration Item

CTE Charge Transfer Efficiency

Dec Declination

DR Data Release

DV Data Validation Pipeline Module

DVA Differential Velocity Aberration

FFI Full Frame Image

FIN FFI Index Number

FITS Flexible Image Transport System

FOV Field of View

FPG Focal Plane Geometry model

KDPH Kepler Data Processing Handbook

KIH Kepler Instrument Handbook

KOI Kepler Object of Interest

MAD Median Absolute Deviation

MAP Maximum A Posteriori

MAST Mikulski Archive for Space Telescopes

MES Multiple Event Statistic

NAS NASA Advanced Supercomputing Division

PA Photometric Analysis Pipeline Module

PDC Presearch Data Conditioning Pipeline Module

PDC-MAP Presearch Data Conditioning Maximum A Posteriori algorithm

PDC-msMAP Presearch Data Conditioning Multiscale Maximum A Posteriori algorithm

PDF Portable Document Format

POC Payload Operations Center

POU Propagation of Uncertainties

PPA Photometer Performance Assessment

ppm Parts-per-million

PRF Pixel Response Function

RA Right Ascension

RMS Root Mean Square

SAP Simple Aperture Photometry

SDPDD Science Data Products Description Document

SNR Signal-to-Noise Ratio

SPOC Science Processing Operations Center

SVD Singular Value Decomposition

TCE Threshold Crossing Event

TESS Transiting Exoplanet Survey Satellite

TIC TESS Input Catalog

TIH TESS Instrument Handbook

TJD TESS Julian Date

TOI TESS Object of Interest

TPS Transiting Planet Search Pipeline Module

UTC Coordinated Universal Time

WCS World Coordinate System

XML Extensible Markup Language